# Type II radio emission predictions: Sources of coronal and interplanetary spectral structure

S. A. Knock and Iver H. Cairns

School of Physics, University of Sydney, Sydney, New South Wales, Australia

Received 28 February 2004; revised 27 August 2004; accepted 26 October 2004; published 7 January 2005.

[1] We extend a model for type II radio bursts to investigate emission from the quiet corona, as well as the emission relating to structures in the corona and interplanetary medium. The most notable effect for the quiet corona is the weakening or disappearance of emission near a peak in the heliocentric Alfvèn speed profile. By inserting various structures into the coronal and interplanetary plasma, most observed type II features are produced. Specifically, multiple-lane events, differing frequency drift rates, emission which turns on and off, and narrowband and broadband emission can be produced.

**Citation:** Knock, S. A., and I. H. Cairns (2005), Type II radio emission predictions: Sources of coronal and interplanetary spectral structure, *J. Geophys. Res.*, *110*, A01101, doi:10.1029/2004JA010452.

## 1. Introduction

[2] Type II radio bursts are associated with propagating shock waves and are characterized by emission which drifts slowly to lower frequency with time. Observations are typically categorized by their wavelength as metric, decametric/hectometric (DH), or kilometric. The dynamic spectra of type II classically consist of two bands of emission separated by approximately a factor of 2 in frequency. The lower-frequency band is interpreted as emission at approximately the local plasma frequency $f_p$, while the upper band is at $2f_p$. Accordingly, type II with metric, DH, and kilometric wavelengths correspond, approximately, to radial distances of $\sim$1–2 $R_\odot$, $\sim$2–10 $R_\odot$, and 10 $R_\odot$, respectively. The typically negative drift rate of these emission bands is ascribed to the motion of the source region away from the Sun, and thus to regions of lower number density and local plasma frequency.

[3] In practice, most observations show the bands to fluctuate dramatically in intensity, bandwidth, and drift rate. Disentangling the details of the underlying physics from the observed spectra is made difficult by features such as a lack of continuous emission, and frequency fine structures such as broadband versus narrowband emission, multiple lanes of fundamental or harmonic emission, and herringbone bursts [e.g., *Roberts*, 1959; *Nelson and Melrose*, 1985; *Cairns and Robinson*, 1987]. It should be noted that there are three subclasses of events which contain multiple bands of fundamental or harmonic emission. The first occur simply as a result of multiple global shocks that each produce type II emission. The second, called multiple-lane events, can have a variety of frequency separations and differing drift rates. They are usually attributed to distinct source regions associated with different portions of the one global shock. The third, known as split-band events, consist of lanes which drift at the same rate with a frequency separation of $\sim$10%. Split-band events are most commonly attributed either to emission from upstream and downstream of the shock or to a plasma processes which results in emission slightly above and slightly below a characteristic frequency [e.g., *Roberts*, 1959; *Smerd et al.*, 1974]. Herringbone bursts each last for a few seconds and occur in groups, and their frequency drift rates have much larger magnitudes ($\gtrsim$ a factor of 10) than the type II backbone. They are not discussed further here.

[4] Only recently have the first in situ observations of a type II source region enabled confirmation and refinement of our understanding of the source of this emission [*Bale et al.*, 1999]. Further, recent observational correlations between pre-existing plasma structures and enhancements in emission levels have highlighted the influence of upstream plasma conditions on the observed spectra [*Reiner et al.*, 1998; *Gopalswamy et al.*, 2001c]. These correlations essentially rely on being able to show that the type II shock and the structure with which it is interacting have a spatial and temporal relation. It is vital to strengthen these characterizations with explicit calculations of the effect such structures have on the observed emission, as performed here.

[5] This paper is the fourth in a series that deals with the development and investigation of a theoretical model for type II radio emission. The four main theoretical components which lead to type II radio emission are (1) electron reflection and acceleration at a shock, via a process known as shock drift acceleration (SDA) [e.g., *Toptyghin*, 1980; *Webb et al.*, 1983; *Holman and Pesses*, 1983; *Wu*, 1984; *Ball and Melrose*, 2001]; (2) the formation throughout the foreshock (Figure 1) of electron beams due to time-of-flight effects [*Filbert and Kellogg*, 1979; *Cairns*, 1986, 1987]; (3) the growth of Langmuir waves driven by electron beams and described by stochastic growth theory (SGT) [*Robinson*, 1992; *Robinson et al.*, 1993; *Cairns and Robinson*, 1997, 1999; *Cairns et al.*, 2000]; and (4) Langmuir wave interaction via nonlinear wave-wave processes, to provide the remotely observed radio emission [*Melrose*, 1985; *Cairns*, 1988;


0148-0227/05/2004JA010452$09.00

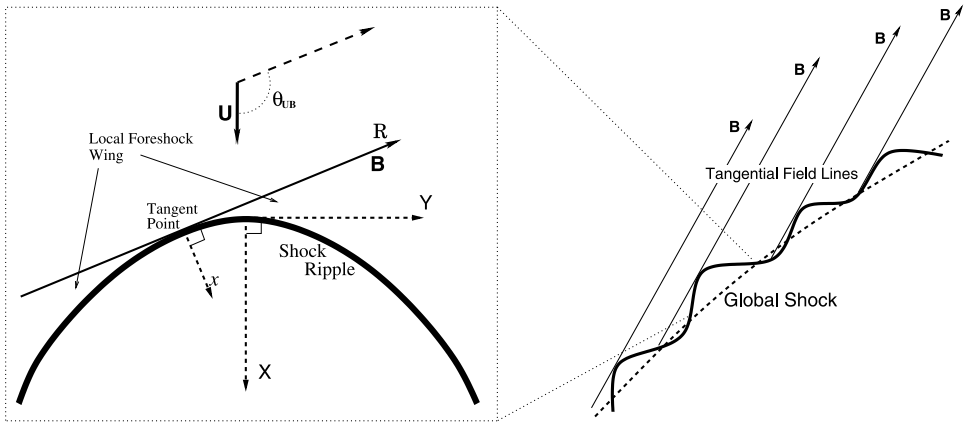


**Figure 1.** Schematic of a two-dimensional slice of a shock ripple, including identification of the tangent point and two local foreshock wings. **B** and **U** are upstream magnetic field and upstream flow speeds, respectively. The two coordinate systems ($R$, $x$) and ($X$, $Y$) are also defined in this figure.

*Robinson and Cairns*, 1993; *Robinson et al.*, 1994]. This model, with appropriate modifications for the specific details, has also been successfully applied to Earth's foreshock [*Kuncic et al.*, 2002], and global merged interaction regions propagating through the outer heliosphere and into the interstellar medium [*Cairns et al.*, 2004; *Mitchell et al.*, 2004].

[6] The first paper [*Knock et al.*, 2001], henceforth referred to as paper 1, developed the basic theoretical model by combining relevant theories for points 1–4 above. These theories had been developed, largely independently, since the discovery of type II some 50 years ago. Paper 1 also made a first tentative comparison with observation, which was found to be in reasonable agreement. A more detailed comparison is currently underway. The second paper [*Knock et al.*, 2003a], henceforth referred to as paper 2, presented a refined version of the model which was used to explore the level of type II emission as a function of plasma and shock parameters. These trends provided theoretical support for a number of observational features, for example the positive correlation between the size and speed of the driving shock wave and the level of emission [see also *Cairns et al.*, 2003]. The third paper [*Knock et al.*, 2003b], henceforth referred to as paper 3, investigated the influence of global shock structure and presented the first theoretically predicted type II dynamic spectra. The calculations of paper 3, which covered a radial distance of $\sim$10 $R_\odot$ to 1 AU, reproduced a number of characteristic type II features, including reasonable emission intensities, bandwidths, and frequency drift rates. Multiple-lane events, resulting from distinct source regions at different heliocentric distances, were also reproduced. It was found that the frequency and temporal structures within a dynamic spectrum depend on observer location, particularly in the fundamental component, due largely to frequency blocking of emission. While small shifts in solar wind and shock parameters can significantly alter the observed emission intensity, random fluctuations ultimately average and lead to relatively smooth continuous dynamic spectra. Therefore it was suggested that coronal and solar wind structures, which are a source of correlated shifts in upstream plasma conditions relevant to emission, as opposed to random fluctuations, should play a major role in the observed structure in type II dynamic spectra.

[7] In the current paper, as with papers 1–3, we aim to provide a theoretical framework which will elucidate the underlying mechanisms relevant to type II radio emission. By extending the calculations of paper 3 into the corona and explicitly incorporating spatial structure into the plasma parameters, a link is made between the diversity in observed spectral morphologies of type II radio bursts and the underlying theory.

[8] The remainder of this paper is structured as follows. Section 2 briefly reviews the model developed thus far, and then describes the specific additions and refinements for the work presented here. Section 3 presents results for emission from a quiet corona and solar wind, emphasizing the effect of a peak in the Alfvèn speed, the importance of lateral expansion of the shock, and difficulties interpreting the frequency drift rate. Section 4 presents the results of introducing large-scale, but localized, plasma structures into the corona and solar wind, emphasizing their effects on intensity and frequency structure in dynamic spectra. Finally, section 5 summarizes the results and outlines some implications for the interpretation of type II observations.

## 2. Type II Model

[9] As mentioned in section 1, the model used here has been developed and presented in detail in papers 1–3 [see also *Cairns et al.*, 2003]. This section begins with a very brief summary of that model. It then outlines modifications to the basic heliocentric models used for the plasma and shock parameters in paper 3, and mentions briefly an issue related to the initial conditions. Finally, an overview is given of how simple plasma structures are incorporated into the corona and solar wind.

### 2.1. Overview of the Model

[10] The foreshock, defined as the region between the shock front and its tangential magnetic field lines, is the source of type II radio emission (Figure 1). Electrons are reflected and accelerated near the magnetic tangent, with

**Table 1.** Summary of Plasma and Magnetic Field Heliocentric Models, as Well as the Gaussian-Distributed Fluctuation About These Models[a]

| Heliocentric Models | Fluctuations (Standard Deviation) |
|---|---|
| $V_{sw}(r) = 4.0 \times 10^5 \left(\frac{r}{AU}\right)^{0.19} - 0.42$ m s$^{-1}$ | ±30% |
| $T_e(r) = 1.5 \times 10^5 \left(\frac{r}{AU}\right)$ K | ±30% |
| $B_1(r) = \sqrt{\left(\frac{B_0 R_\odot^2}{r^2}\right)^2 + \left(B_0 \frac{2\pi}{T} R_\odot^2 V_{gs} r\right)^2}$, $B_0 = 1.8 \times 10^{-4}$ T | ±10% |
| $\theta_{BV_{sw}}(r) = 2\pi - \tan^{-1}\left[\frac{2\pi r}{T V_{SW_R}}\left(1.0 - \frac{R}{r}\right)\right]$ | ±50% |
| $b_{gs}(r) = r^{-1}\left(\frac{r}{AU}\right)^{-0.3}$ m$^{-1}$, $X_H = r - b_{gs} Y_H{}^2$ | ±0% |
| $\kappa = 2.5$ | ±30% |
| $N_e(r)$, see equation (2) | ±20% |
| $T_i(r)$, see equation (3) | ±30% |
| $b(r)$, see equation (4) | ±20% |

[a]Here $r$ refers to radial distance, and the subscripts *sw* and *gs* refer to the solar wind and global shock, respectively. The symbol $T$ in the equations for $B_1(r)$ and $\theta_{BV_{sw}}(r)$ is the solar rotation period.

beam distributions subsequently forming via time-of-flight effects. This physics is treated using Liouville's theorem and conservation of magnetic moment in the deHoffman-Teller frame. The electron beams constitute a source of free energy for the growth of Langmuir waves, which undergo nonlinear interactions to produce freely propagating radio emission. This physics is treated using marginal stability, the convective derivative of available free energy, and the known nonlinear conversion efficiencies from Langmuir waves to radiation. Since more details are given in papers 1 and 2, they are not repeated here.

[11] A global parabolic shock is defined to consist of many small ripples (Figure 1), whose scales are determined by the local magnetic correlation length. The shock has an equatorial trajectory with ripples packed on the one-dimensional slice of the shock surface which lies in the equatorial plane. Cylindrical symmetry is then employed to form a global three-dimensional shock front. The calculation of the emission from each ripple is performed using the local plasma and magnetic field variables. Relevant quantities include $N_e$, $V_{sw}$, $T_e$, $T_i$, $B$, the magnetic field orientation $\theta_{BU}$, and the level of nonthermal electrons, which is parameterized by $\kappa$, the exponent of the electron distribution function's asymptotic velocity dependence $f(v) \propto v^{-(\kappa+1)}$. The radial dependence of the plasma parameters is determined by analytic heliocentric models, which were discussed in paper 3 and are summarized in Table 1. Additionally, Gaussian-distributed fluctuations are imposed on these radial variations to achieve a more realistic model solar wind. Type II dynamic spectra are then produced by summing over the emission from individual ripples at progressive time steps.

[12] The type II physics of electron acceleration and beam formation, as well as subsequent emission processes, are independent of what causes the shock. The only influences that a particular shock driving mechanism has on the observed dynamic spectra are from the acceleration and continued propagation of the shock. In regard to a shock's acceleration, blast wave shocks should have a very rapid, almost instantaneous, initial acceleration and most likely a relatively quick deceleration due to the lack of a continued source of driving energy. However, observations of CMEs show that they, and thus their associated shock waves, continue to accelerate through the corona before subsequently decelerating as they propagate through the solar wind. In regard to a shock's continued propagation, encountering a peak in the heliocentric Alfvèn speed $V_A$ profile can lead to a weakening of the shock, potentially preventing its propagation to greater radial distances and lower emission frequencies. With these points in mind, it should be noted that the calculations of this paper begin by turning on the shock with a given speed, similar to a blast wave. However, the shock's propagation, irrespective of any intermediate weakening, is allowed to continue. Further, a slight deceleration is incorporated, based on observations of CMEs [*Gopalswamy et al.*, 2001a].

### 2.2. Changes to the Model

[13] In order to extend the calculations of paper 3 into the corona, some of the heliocentric models needed to be refined. Specifically, this paper includes different heliocentric models for electron number density $N_e$, ion temperature $T_i$, and ripple curvature, parameterized by $b$. Further, the ability to modify the flow speed, and thus the strength, of the flanks of the global shock was incorporated, in order to capture the effects of lateral expansion.

[14] In the dynamic spectra calculations presented in this paper, the heliocentric dependence of $N_e$ takes the form [*Saito et al.*, 1977]

$$N_e(r) = a_1 \left(\frac{r}{R_\odot}\right)^c + a_2 \left(\frac{r}{R_\odot}\right)^d, \quad (1)$$

where, $a_1 = 1.36 \times 10^{12}$ m$^{-3}$, $a_2 = 1.68 \times 10^{14}$ m$^{-3}$, $c = -2.14$, and $d = -6.13$ are the values which fit to the equatorial background. The motivation for changing the heliocentric model for $N_e$, from that used in paper 3, is twofold. First, the model of *Saito et al.* [1977] is more widely used in the literature, particularly in observational analyses relating frequency drift rates to shock speeds. Second, the combination of the Saito $N_e$ model and the Parker spiral magnetic field strength produce a peak in $V_A$ at approximately 3–4 $R_\odot$. Accordingly, using this combination of models enables us to predict the observable effects on type II spectra should such a peak exist. It should be noted that the different power laws followed by $N_e$ in a number of other models, for example the one we previously used, based on type III observations, does not produce a peak away from the solar surface; this can be seen in Figure 4 in section 3.1 and is discussed further in section 3.

[15] The heliocentric model for $T_i$ in this paper's calculations takes the form

$$T_i(r) = 0.5 \times 10^5 \left(\frac{r}{AU}\right)^{-0.67}, \quad (2)$$

in units of K, where $r$ is the radial distance. The change in exponent, relative to that used in paper 3, for the heliocentric dependence of $T_i$ was to more closely match observational evidence that implies coronal $T_i$ is often equivalent to or exceeds the electron temperature $T_e$; this is converse to the situation in the solar wind in which $T_e$ typically exceeds $T_i$. In paper 3, $T_i$ had the same radial dependence as $T_e$.

[16] In this paper, as in our previous work, the ripple curvature $b$ is based on the magnetic correlation length $\langle l \rangle$. Previously, we used the observational values at 1 AU

obtained by *Collier et al.* [2000] and assumed a heliocentric dependence based on the scale length of electron density fluctuations given by *Robinson and Cairns* [1998]. This is a reasonable approximation in the solar wind but becomes rapidly worse closer to the Sun. In contrast, a flux tube model for $\langle l(r)\rangle$ agrees well with observations from low heliocentric distances to 1 AU [*Hollweg et al.*, 1982; *Mancuso and Spangler*, 1999; *Collier et al.*, 2000]. Therefore, in this work, we use a ripple curvature given by

$$b = \langle l\rangle^{-1} = 7.3 \times 10^{-6}\sqrt{B_1}m^{-1}, \quad (3)$$

where $B_1(r)$ is the equatorial magnetic field strength given by Parker's model.

[17] Previously, the flow speed $U_{\hat{n}}$ normal to the global shock was considered to be the same across the entire shock front. This was reasonable for a large shock front in the interplanetary medium. However, for our purposes here it is useful to be able to change between an expanding shock and one which only sees an upstream flow aligned with the axis of the parabola, as is the case in the ripple calculations. Thus here the flow speed $U_{\hat{n}}$ used for the calculation of emission from a ripple is

$$U_{\hat{n}} = U_{gs}\left(\cos\alpha_{gs} + \varepsilon - \varepsilon\cos\alpha_{gs}\right) - V_{sw}\cos\left(\theta_r - \alpha_{gs}\right), \quad (4)$$

where (see Figure 2) $\theta_r$ is the angle between the solar wind flow direction (radial from the Sun) and the axis of the global parabolic shock front, $\alpha_{gs}$ is the angle between a tangent to the global shock front and a line perpendicular to the global shock axis (i.e., tangent to the global shock's leading edge), and $\varepsilon$ selects between no expansion and full expansion, corresponding to values between 0 and 1, respectively. It should be noted that the size of the parabola ($b_{gs}$) defining the global shock and the rate of expansion ($\varepsilon$) are not necessarily tied to one another.

### 2.3. Incorporating Structure

[18] Simple representations of solar wind and coronal structures are incorporated into the calculations presented here by defining spatial regions in which the plasma and magnetic field variables are modified relative to the values predicted by the heliocentric models. Relevant quantities include $N_e$, $V_{sw}$, $T_e$ and $T_i$, $B$, magnetic field orientation $\theta_{BU}$, and $\kappa$ which parameterizes the level of nonthermal electrons.

[19] We have defined spatial regions that are qualitatively similar to common coronal and solar wind structures and imposed changes in plasma and magnetic quantities representative of the structures they are mimicking. Specifically, three types of spatial regions, which are defined only by their two dimensional cross section, are considered: (1) circular regions, which can be considered to be either crude approximations to the magnetic clouds of slower pre-existing CMEs or simply fluctuations in the solar wind plasma conditions on spatial scales larger than those imposed on the heliocentric models; (2) spiral regions, defined to lie between spiral arms emanating from the Sun (these regions consist of three subregions where variables are modified in accordance with the typical profiles of corotating interaction regions (CIRs) [e.g., *Mann et al.*, 2002]); and (3) horseshoe shaped regions connected to the Sun that are intended to mimic coronal loops.

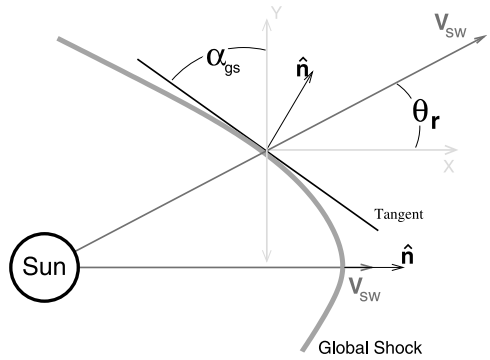


**Figure 2.** A schematic depicting the angles $\alpha_{gs}$ and $\theta_r$ relevant to equation (4). $\mathbf{V}_{sw}$ and $\hat{\mathbf{n}}$ represent solar wind direction (radial from the Sun) and global shock normal, respectively. The faint shaded X and Y axes are parallel those of the global parabolic shock.

It should be noted that none of these structures are currently endowed with realistic internal structure, but instead are simple first approximations. Even so, they provide useful insights into the sort of correlations one should expect between specific plasma structures and observed dynamic spectra.

## 3. Predictions for Shocks Moving Through a Quiet Corona and Solar Wind

[20] This section investigates the nominal case of a quiet corona and solar wind in which the only variation in plasma and magnetic variables from the values predicted by the heliocentric models are Gaussian-distributed fluctuations. The calculations presented in this section are for a shock initialized at a heliocentric distance of 1.1 $R_\odot$. Calculations are stopped when the shock reaches 1 AU (Figure 3a). In each calculation a deceleration $a_{gs} = 5.4 \times 10^{-6}U_{gs} - 2.193$ m s$^{-2}$ is incorporated, consistent with *Gopalswamy et al.* [2001a]. Other relevant parameters can be found in Table 1 and the captions of Figure 3 and of Figure 5 in section 3.2.

[21] The Alfvèn speed $V_A$ plays a vital role in the formation and strength of fast mode collisionless shocks, and thus in predictions for type II emission [*Mann et al.*, 1999; *Gopalswamy et al.*, 2001b; *Mann et al.*, 2003]. For a given shock speed, different heliocentric profiles in $V_A$ should influence the wavelength domains for which a type II will be observable (above the detection threshold): for example, a relatively strong type II could weaken, even turning off, as the shock approaches a peak in the $V_A$ profile and weakens (thereby reflecting fewer electrons), only to strengthen as the local $V_A$ decreases again at larger heights. Naturally, if $V_A$ is higher than the speed of the propagating disturbance, then no fast mode shock will form, and thus no type II emission should be possible. It should be remembered that, based on the findings of paper 2, a shock propagating at less than twice $V_A$ is ineffective at reflecting and accelerating electrons capable of producing significant radio emission. Previous workers [e.g., *Mann et al.*, 1999; *Gopalswamy et al.*, 2001b; *Mann et al.*, 2003] have discussed, qualitatively, the effect of a peak in the $V_A$ profile on type II emission. Here we provide an explicit quantitative

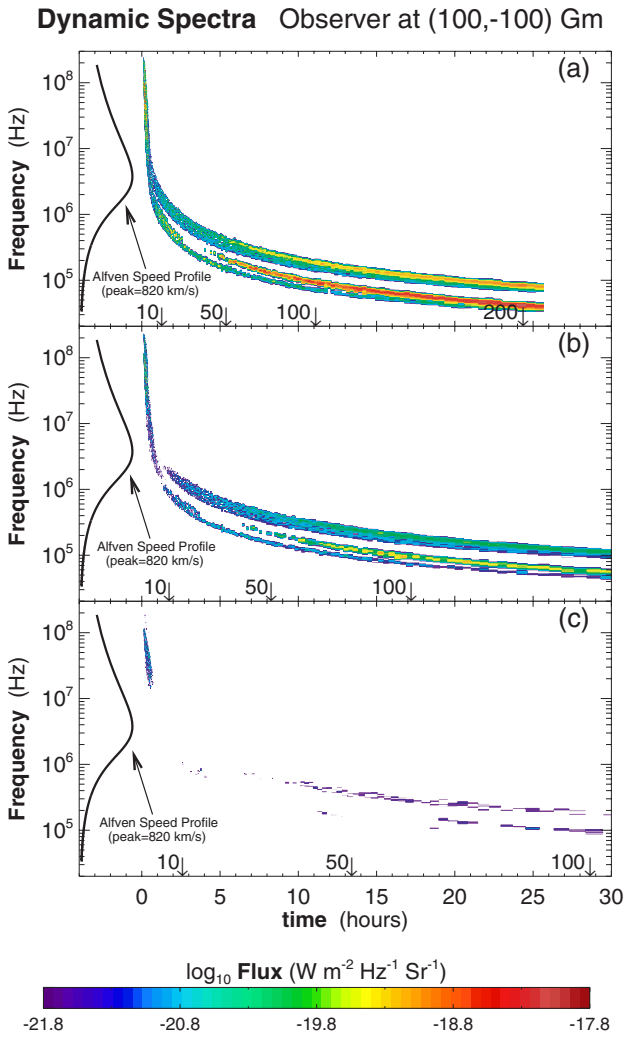


**Figure 3.** Dynamic spectra of type II bursts from a quiet corona and interplanetary medium. The heliocentric Alfvèn speed profile is plotted as a function of fundamental frequency. (a) $U_{gs}$ = 2000 km s$^{-1}$, (b) $U_{gs}$ = 1300 km s$^{-1}$, and (c) $U_{gs}$ = 800 km s$^{-1}$. For each spectrum the times corresponding to radial heights of 10, 50, 100, and 200 solar radii are indicated.

calculation of the type II burst dynamic spectra associated with a given $V_A$ profile.

### 3.1. Effects Due to the Alfvèn Speed Profile

[22] Figure 3 presents dynamic spectra which, as in the rest of the calculations presented in this paper, uses the $N_e$ model of *Saito et al.* [1977]. This model was chosen for both the presence of a $V_A$ peak and the fact that it produces values of $N_e$ in reasonable agreement with those observed, from the corona to 1 AU. A weakening of emission is clearly seen, in Figure 3, over the range of frequencies corresponding to the peak in $V_A$. The diminution is more noticeable for slower shocks, with emission turning off entirely for a shock propagating at or below the $V_A$ peak (Figure 3c). That is, this theory clearly predicts that a spatial peak in $V_A$ can cause a type II burst to turn off and then on again at lower frequencies.

[23] The existence or not of a break in the type II burst, and the degree of diminution, depends upon the details of the $V_A$ profile and the shock speed. For calculations of significantly faster shocks, there is often little or no weakening, despite the presence of a peak in $V_A$, while slower shocks tend to weaken and turn off over larger frequency ranges.

[24] In order to quantify this effect, we briefly consider four models for $N_e$ and their implications for the $V_A$ profile near the Sun. Of the four models considered, two are based on white-light data and widely used in the literature: the *Newkirk* [1961] model with

$$N_e(r) = N_0 \times 10^{4.32/(\frac{r}{R_\odot})} \tag{5}$$

and $N_0 = 4.2 \times 10^4$ m$^{-3}$, and equation (1) [*Saito et al.*, 1977]. The other two [*Reiner et al.*, 1998; *Robinson and Cairns*, 1998] are power law fits to an observation of a type II burst,

$$N_e(r) = 23 \times 10^6 \left(\frac{r}{AU}\right)^{-2.86} m^{-3}, \tag{6}$$

and observations of type III bursts,

$$N_e(r) = 7.0 \times 10^6 \left(\frac{r}{AU}\right)^{-2.19} m^{-3}, \tag{7}$$

respectively. The model used in paper 3 is that of *Robinson and Cairns* [1998]. It should be noted that the Robinson and Cairns density model is of questionable validity below a few $R_\odot$, due to its derivation assuming $r \gg R_\odot$. Equation (7) is similar to the first term in equation (1); this suggests a relatively straightforward hybridized model combining equation (7) and the second term in equation (1). While the resultant model would be similar to that of *Saito et al.* [1977], it has the useful property that the term which dominates the density in interplanetary space is normalized to a 1 AU value while the term which dominates the coronal density is normalized to a coronal value. Nevertheless, the *Saito et al.* [1977] model is used below.

[25] Here only one magnetic field strength profile is considered, that of an equatorial Parker spiral. However, it should be remembered that different $B$ profiles will lead to similar effects on $V_A$ as the different density profiles. The four resulting $V_A$ profiles are shown in Figure 4. Newkirk's model produces a $V_A$ profile which peaks between 2 and 3 $R_\odot$ at ~400 km s$^{-1}$. *Saito et al.*'s [1977] model also produces a peak; however, it is centered between 3 and 4 $R_\odot$ with a peak height ~850 km s$^{-1}$. Neither of the other models [*Reiner et al.*, 1998; *Robinson and Cairns*, 1998] result in a $V_A$ peak above the solar surface.

[26] In the current context, what is important is the implications these four $V_A$ profiles have for type II emission. Therefore, assuming other relevant conditions are favorable and remembering that shocks with speeds less than twice $V_A$ are unlikely to produce observable emission (paper 2), what follows is a summary of the speed constraints on observable type II emission for the $V_A$ profiles shown in Figure 4. For the Newkirk and Saito density models, the lowest and highest minimum speeds within the metric, DH, and kilometric wavelength domains are quoted. Since neither of the other two models [*Reiner et al.*, 1998; *Robinson and Cairns*,

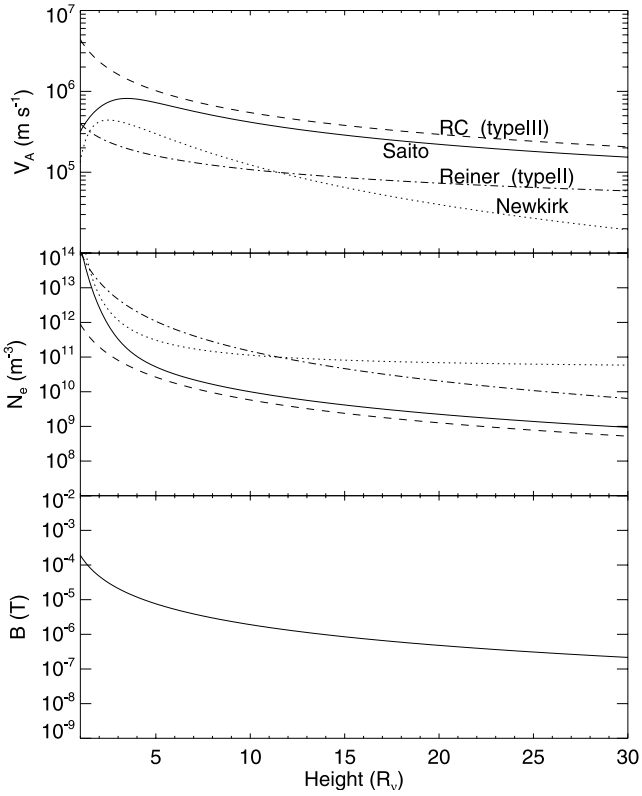


**Figure 4.** (top, middle) Spatial profiles of the Alfvèn speed and electron number density for the four different density models discussed in the text. (bottom) Spatial profile of the equatorial magnetic field strength given by Parker's model.

1998] produces a peak in $V_A$, only the highest minimum speed of the wavelength domains are quoted.

[27] Using Newkirk's density model the type II theory implies that an observable metric type II requires a shock speed (where ranges in the wavelength domains are quoted) $U \gtrsim 200-800$ km s$^{-1}$, while observable DH bursts require $U \gtrsim 200-900$ km s$^{-1}$, and observable kilometric bursts could be produced by $U \gtrsim 600-1300$ km s$^{-1}$ km s$^{-1}$, for the plotted region. It should be noted that Newkirk's model is not considered valid above 30 $R_\odot$, and thus the situation in which a strong shock can form for a disturbance traveling $\sim$100 km s$^{-1}$ and drive kilometric emission probably does not occur in practice. Saito's density model with its higher $V_A$ peak requires $U \gtrsim 600-1300$ km s$^{-1}$ in order to drive significant metric emission, with $U \gtrsim 1000-1700$ km s$^{-1}$ required for significant DH emission, and $U \gtrsim 400-1000$ km s$^{-1}$ for kilometric emission from the plotted region. For the *Reiner et al.* [1998] and *Robinson and Cairns* [1998] density models, metric emission requires $U$ 800 and 8000 km s$^{-1}$, respectively, while DH requires $U$ 600 and 5000 km s$^{-1}$, and kilometric requires $U$ 200 and 1100 km s$^{-1}$, respectively. This shows quite clearly that differing heliocentric models for $N_e$, and also $B$, can lead to significant restrictions on the speed at which a disturbance is required to propagate in order to produce significant type II radio emission.

[28] Significant differences in the required driving speeds for type II emitting shocks are clearly evident in the above discussion. Remembering that all four of the $N_e$ models considered have their basis in observation, it is apparent that the variability of plasma conditions near the Sun has considerable implications for the relationship between shock speed and type II emission. Specifically, it implies that spatial and temporal variations in $N_e$, $B$, and $V_{sw}$, due to unusual solar activity, positionally related phenomena such as the slow (equatorial) versus the fast (polar) wind, or periodic fluctuations like the solar cycle, need to be taken into account when interpreting statistical relationships between type II emission and shock speed.

### 3.2. Effects Due to Lateral Expansion

[29] In a quiet corona, the magnetic field is essentially radial in Parker's solar wind model, and thus a radially propagating shock is quasi-parallel. As shown in paper 2, quasi-parallel shocks do not generate significant type II emission. Therefore the type II emission from a parabolic shock in a quiet corona should be dominated by the quasi-perpendicular flanks of the shock. In order for the flanks of the shock to be strong enough to reflect and accelerate electrons capable of driving type II emission, the propagating disturbance needs to be expanding laterally. This is due to the shock strength being strongly dependent on the normal component of the flow speed of the shock.

[30] Thus the lateral expansion of the shock wave determines the heliocentric extent of the source region close to the Sun and in the absence of magnetic structures. In the situation of a strong lateral expansion this leads to very broadband type II emission, to the extent that it can be difficult to distinguish between the fundamental and harmonic frequency bands. Specifically, the case shown in Figure 5b is for a shock which expands as rapidly as it rises through the corona. This produces emission which is so broadband that the upper edge of the fundamental band is at a higher frequency than the lower edge of the harmonic frequency band. Alternatively, the case shown in Figure 5a is for a shock with no significant lateral expansion. This means emission isn't dominated by the legs/flanks of the shock, leading to an emission region of limited radial extent, and thus a narrowband type II. However, for nominal coronal parameters, this significantly weakens the emission, thus requiring optimized parameters to produce strong narrowband emission. Such optimal parameters occur for certain coronal structures (e.g., for loop structures, as shown in section 4), implying they are probably the dominant source of intense narrowband metric type II emission.

[31] The lower frequency edge of the emission in Figure 5 drifts at a rate which coincides with that of the shock's leading edge, shown by the two lines labeled "fundamental" and "harmonic." However, this is not always the case: For a weaker burst or a higher minimum intensity, the lower frequency edge often drifts at a rate which is noticeably slower than that of the shock's leading edge. This is partly due to the $V_A$ profile and partly due to the magnetic field orientation near the shock's leading edge. The higher frequency edge drifts slowly due to the shock's lateral expansion, and thus the lower radial speed of the base of the shock's flanks.

[32] One aspect of the broadband nature of the type II emission generated by a strongly expanding shock is the apparent velocity determined via the frequency drift rate.

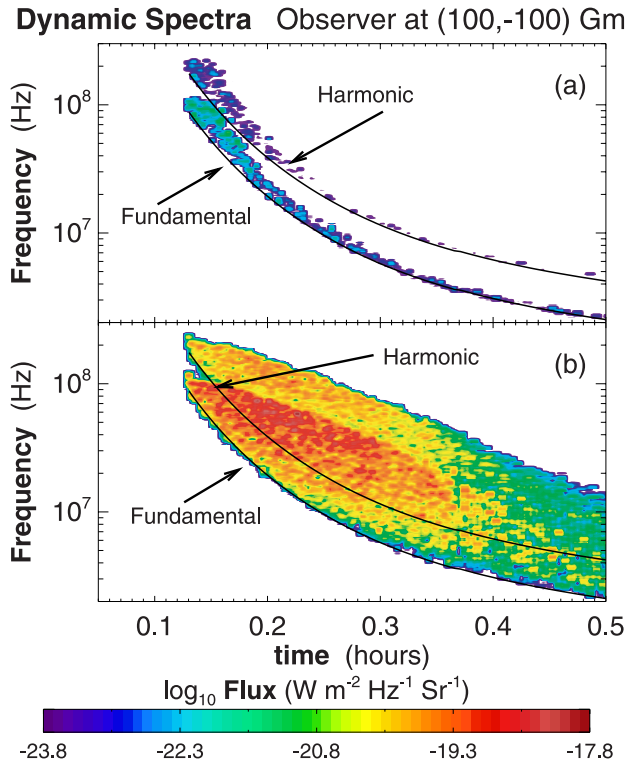


**Figure 5.** Dynamic spectra for type II bursts from a quiet corona. The two curves in each panel indicate the fundamental and harmonic frequency drift rate of the shock's leading edge. The only difference in the initial conditions is that in Figure 5a the shock has no significant lateral motion, that is $\varepsilon = 0$, while in Figure 5b the shock is expanding at its radial speed, that is $\varepsilon = 1$.

The apparent drift rate is drastically reduced due to emission being dominated by regions of the shock that move primarily laterally, through plasma with relatively constant $f_p$. Such situations make determination of the shock speed based on frequency rate very difficult, with an estimation based on the center frequency of the emission band highly erroneous. A better approach would be to consider the drift rate of the lower frequency edge of the emission, as in the absence of structure this should track most closely the leading edge of the emission region, which one would expect to consist primarily of a radial component of motion, as in Figure 5. However, as mentioned above, this can also have problems when a $V_A$ peak exists or the conditions for emission from the shock's leading edge are otherwise unfavorable. It is clear that interpretation of frequency drift rates in terms of a simple shock speed, and even fundamental versus harmonic bands, is fraught with difficulty.

## 4. Predictions for Shocks Moving Through a Structured Corona and Solar Wind

[33] Observations suggest [e.g., *Reiner et al.*, 1998; *Gopalswamy et al.*, 2001c], and theory predicts (paper 3) [see also *Cairns et al.*, 2004] that type II dynamic spectra depend strongly on upstream plasma and magnetic field conditions, notably $T_e$ and the magnetic field orientation. This section explores some possible manifestations of coronal and solar wind structure, such as coronal loops, CIRs, and magnetic clouds. The calculations presented in this section are for a shock initialized at a heliocentric distance of 1.1 $R_\odot$ with a speed $U_{gs}$ = 1100 km $s^{-1}$. A deceleration $a_{gs} \approx 3.2$ m $s^{-2}$ is incorporated, as per *Gopalswamy et al.* [2001a]. The shock is considered to be expanding below its radial speed, with $\varepsilon = 0.5$. Other relevant parameters can be found in Tables 1 and 2.

### 4.1. Coronal Structure

[34] As mentioned above, the primary structure which we are trying to mimic in the solar corona is that of coronal loops. Those with high temperature and density relative to the background corona, based on papers 2 and 3 and the calculations presented below, should provide a source of enhanced emission that should be clearly visible in radio dynamic spectra. In contrast (not shown here), relatively cool dilute loops should lead to relative voids in dynamic spectra.

[35] Figure 6 shows the plasma parameters and the predicted fundamental and harmonic emission as a function of location. The parameters inside the spatial structures are modified from the heliocentric model values. Details of the modifications to plasma and magnetic field parameters in spatial structures are given in Table 2.

[36] Figure 7 is the dynamic spectrum predicted for the structures in Figure 6, as seen by an observer at $(X_H, Y_H)$ = (100, −100) Gm, which is a position approximately 1 AU from the center of the Sun. Emissions are labeled as either fundamental or harmonic. The frequency drift rates of the fundamental and harmonic emission at the leading edge of the shock wave are also shown.

[37] By adding and removing the imposed spatial structures, as well as separating the fundamental and

**Table 2.** Description of Modifications to the Plasma and Magnetic Field Variables Within the Regions of Imposed Spatial Structure[a]

| | Structures | | | | | |
|---|---|---|---|---|---|---|
| Quantity | $Loop_1$ | $Loop_2$ | $Cloud_1$ | $Cloud_2$ | $CIR_1$ | $CIR_2$ |
| $(X, Y)$, Gm | (0.65, −0.3) | (0.65, 0.25) | (40, −10) | (70, −30) | upper | lower |
| $T_e$ | ↑80% | ↑190% | ↑70% | 0% | ↑200%; ↑60%; ↑20% | ↑300%; ↑90%; ↑30% |
| $T_i$ | ↑60% | ↑100% | ↑30% | ↓30% | ↑100%; ↑30%; ↓10% | ↑100%; ↑30%; ↓10% |
| $B_1$ | ↓40% | ↑30% | ↓15% | ↑100% | ↑180%; 0%; ↓30% | ↑180%; 0%; ↓30% |
| $V_{SWR}$ | ↓100% | ↓100% | ↓30% | ↑30% | ↑104%; ↑40%; ↑13% | ↑56%; ↑14%; ↑7% |
| κ | ↑20% | ↓30% | ↓30% | ↑10% | ↓30%; ↓30%; ↑30% | ↓30%; ↓30%; ↑30% |
| $N_e$ | ↑300% | ↑130% | ↑70% | ↑50% | ↑40%; ↑40%; ↓40% | ↑50%; ↑50%; ↓50% |
| θ | loop-aligned | loop-aligned | ↓25% | ↓10% | ↓10%; ↓10%; ↓10% | ↓10%; ↓10%; ↓10% |

[a]These modifications are relative to the values determined by the heliocentric models outlined in Table 1 and section 2.

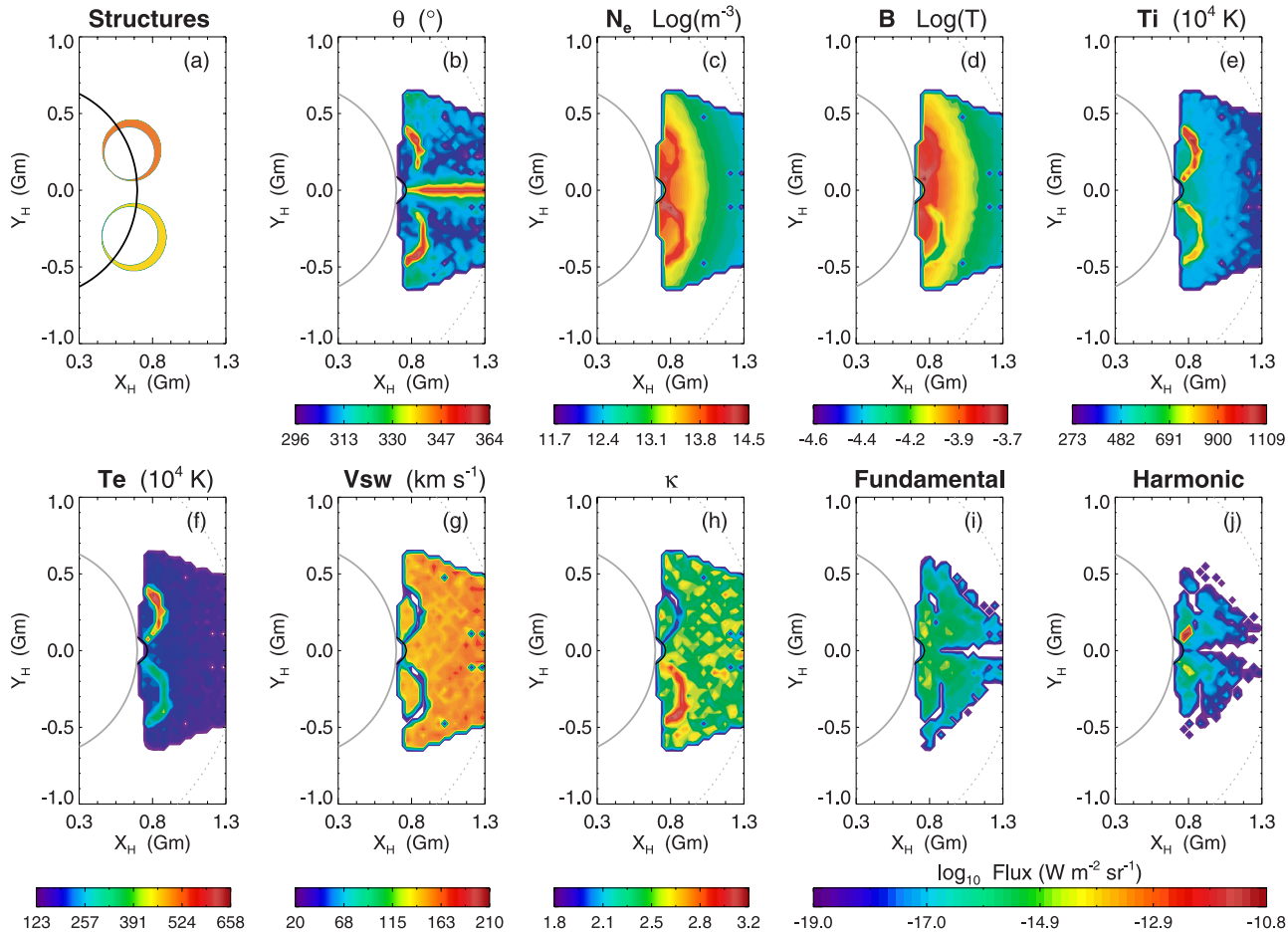


**Figure 6.** (a) Structures defined in the corona; (b) angle θ between the magnetic field and the local normal for the global shock; (c) electron number density $N_e$; (d) magnetic field strength $B$; (e) ion temperature $T_i$; (f) electron temperature $T_e$; (g) solar wind speed $V_{sw}$; (h) level of nonthermal electrons, parameterized by κ; (i) received, frequency integrated, fundamental emission as a function of location; and (j) received, frequency integrated, harmonic emission as a function of location. The semi-circle in each panel denotes the solar surface, and the small black parabola, centered on $Y_H = 0$, is the initial shock.

harmonic components of the emission, the source of spectral features can be easily identified. In Figure 7 the emission from the background plasma is dominated by fundamental emission while the loop-related emission is dominated by harmonic emission. The highest frequency band corresponds to harmonic emission from the loop in the negative $Y_H$ region of Figure 6. The next highest frequency band and most intense emission in the spectrum, due largely to the harmonic emission's stronger dependence on $T_e$, is harmonic emission from the loop in the positive $Y_H$ region of Figure 6. The intensification of emission from this loop does not occur for the entire loop due to unfavorable magnetic field orientation near the loop's apex. The weak patches of emission, extending over a similar time period, at a slightly lower frequency (just below the dashed line) are fundamental emission from the loop in the negative $Y_H$ region, while the loop in the positive $Y_H$ region fails to produce significant fundamental emission.

[38] The large region of emission extending from 0.13 to 0.43 hours and from ∼100 down to ∼15 MHz is entirely composed of fundamental emission from the background plasma, even though a large fraction of it lies above the harmonic frequency for the shock's leading edge. The splitting of this emission into two regions is a result of emission from the two loops being shifted to higher frequencies, thereby leaving relative voids in the dynamic spectrum, that somewhat resembles a split-band type II burst.

[39] The differences in duration of the gap in the background fundamental emission relative to the loop-related emission is due to the loop's magnetic field orientation being quasiparallel to the shock front beyond time $t \simeq$ 0.2 hours. This decrease is expected based on the $\theta_{UB}$ dependence of emission in paper 2.

[40] It is interesting to notice that observers might easily mistake the harmonic background emission, that is, the weak patches between 0.19 and 0.32 hours and from ∼200 down to ∼100 MHz, for a continuation of the fundamental emission from the higher density loop structure. This illustrates the difficulty in distinguishing fundamental from harmonic emission, based on frequency alone, in a structured source region.

[41] It should be noted that while the specific example shown here leads to an increase in the intensity of harmonic emission associated with the structures, both

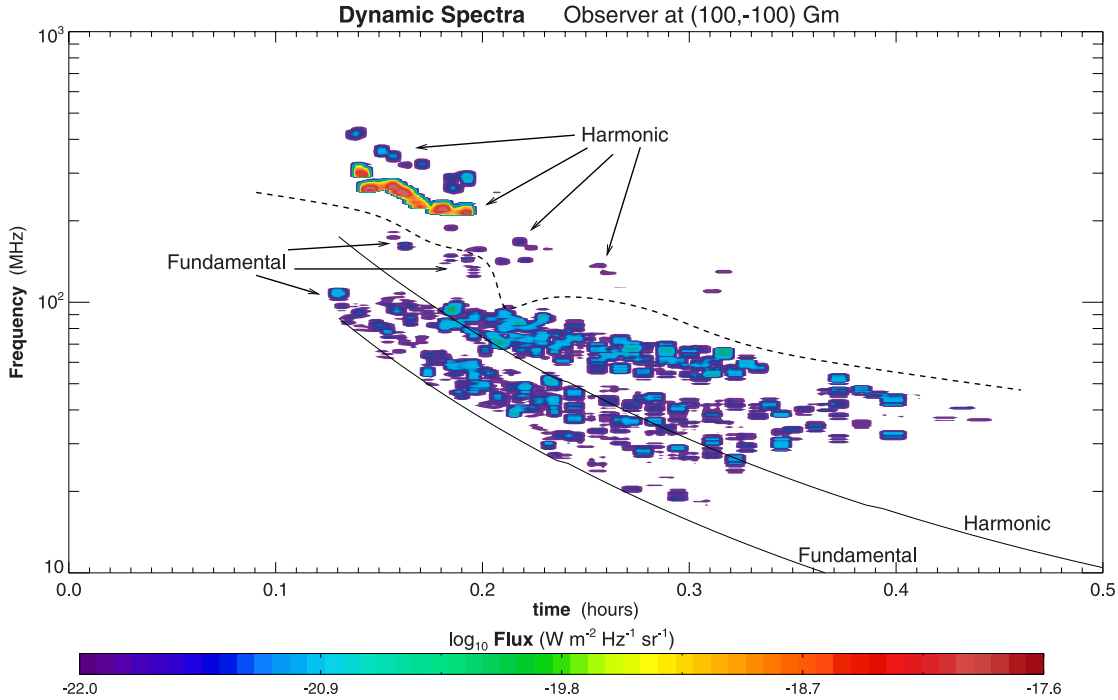


**Figure 7.** Dynamic spectrum of a metric type II burst from a structured corona; the two solid curves are the fundamental and harmonic frequency drift rate of the shock's leading edge. The dashed line separates the predicted fundamental (below) and harmonic (above) emission.

increases and decreases in either fundamental or harmonic emission are possible. Predicted variations in emission due to variations in $N_e$, $T_e$, $T_i$, $\theta_{UB}$, $\kappa$, $U$, and $B$ are described in detail in paper 2.

### 4.2. Interplanetary Structure

[42] Here we present the dynamic spectra predicted for two types of solar wind structure, namely, spiral bounded regions which mimic CIRs and circular regions which crudely mimic the magnetic clouds of slow pre-existing CMEs.

[43] Figure 8 shows the plasma parameters, the location of the structures, and the fundamental and harmonic fluxes as a function of location. There are two structures which mimic CIRs. The upper one remains in the positive $Y$ region of the plots while the lower one lies close to the $X$ axis, crossing into the negative $Y$ region of the plots beyond about $X = 70$ Gm. The location of the observer is marked with a star in the lower right corner of the fundamental and harmonic emission plots.

[44] The various manifestations of the plasma structures in Figure 8 can be seen in the predicted dynamic spectrum (Figure 9). Discussion here focuses on the DH-kilometric emission beyond $t \simeq 2$ hours, since Figure 7 shows the higher-frequency emission in detail. Apparent in Figure 9, as in Figure 3, is the drop in emission associated with the peak in $V_A$.

[45] This dynamic spectrum extends over 33 hours, corresponding to the shock's propagation from 1.1 $R_\odot$ to a radial distance of approximately 93 Gm ($\sim$130 $R_\odot$). Beyond $t \simeq 33$ hours, emission from the shock, now traveling at $\sim$650 km $s^{-1}$, drops below $\sim 10^{-22}$ W $m^{-2}$ $Hz^{-1}$ $sr^{-1}$ (1 sfu).

[46] Emission due to the background plasma begins at about 1 MHz in both the fundamental and harmonic bands, starting at $t \simeq 2$ and 4 hours, respectively. This emission follows fairly closely the frequency drift of the shock's leading edge and weakens to insignificant levels beyond $t \simeq$ 17 hours.

[47] The most intense emission in the DH-kilometric range, reaching a peak of approximately $10^{-18}$ W $m^{-2}$ $Hz^{-1}$ $sr^{-1}$, is that associated with the cloud structure located at $(X, Y) = (40, -10)$ Gm in Figure 8. Here the increased emission is primarily due to the low $\kappa$ and high $T_e$ for fundamental and harmonic components, respectively.

[48] Most of the rest of the discernible structure in the dynamic spectrum is a result of the two CIR-like structures. Visible in its harmonic component, the source region due to the upper CIR produces the very narrow, highest frequency, emission lane. This lane drifts at a rate similar to the leading edge, though at a higher frequency due to the source region's position on the flank of the shock being at a smaller heliocentric distance. The lower CIR produces an emission lane at a slightly lower frequency which drifts faster than the leading edge drift rate prior to $t \simeq 18$ hours. This is due to the source region moving up the flanks of the shock, toward the shock's leading edge. As the curvature of the CIR takes it across the $X$ axis at $X \simeq 75$ Gm the source region starts moving away from the leading edge, causing the frequency drift rate beyond $t \simeq 18$ hours to drop below that of the leading edge.

[49] The fundamental emission associated with the CIRs is absent due to frequency blocking prior to $t \simeq 18$ hours, when both CIRs are on the far side of the global shock. Beyond $t \simeq 18$ hours the fundamental emission associated with the lower CIR becomes visible, drifting at a rate below

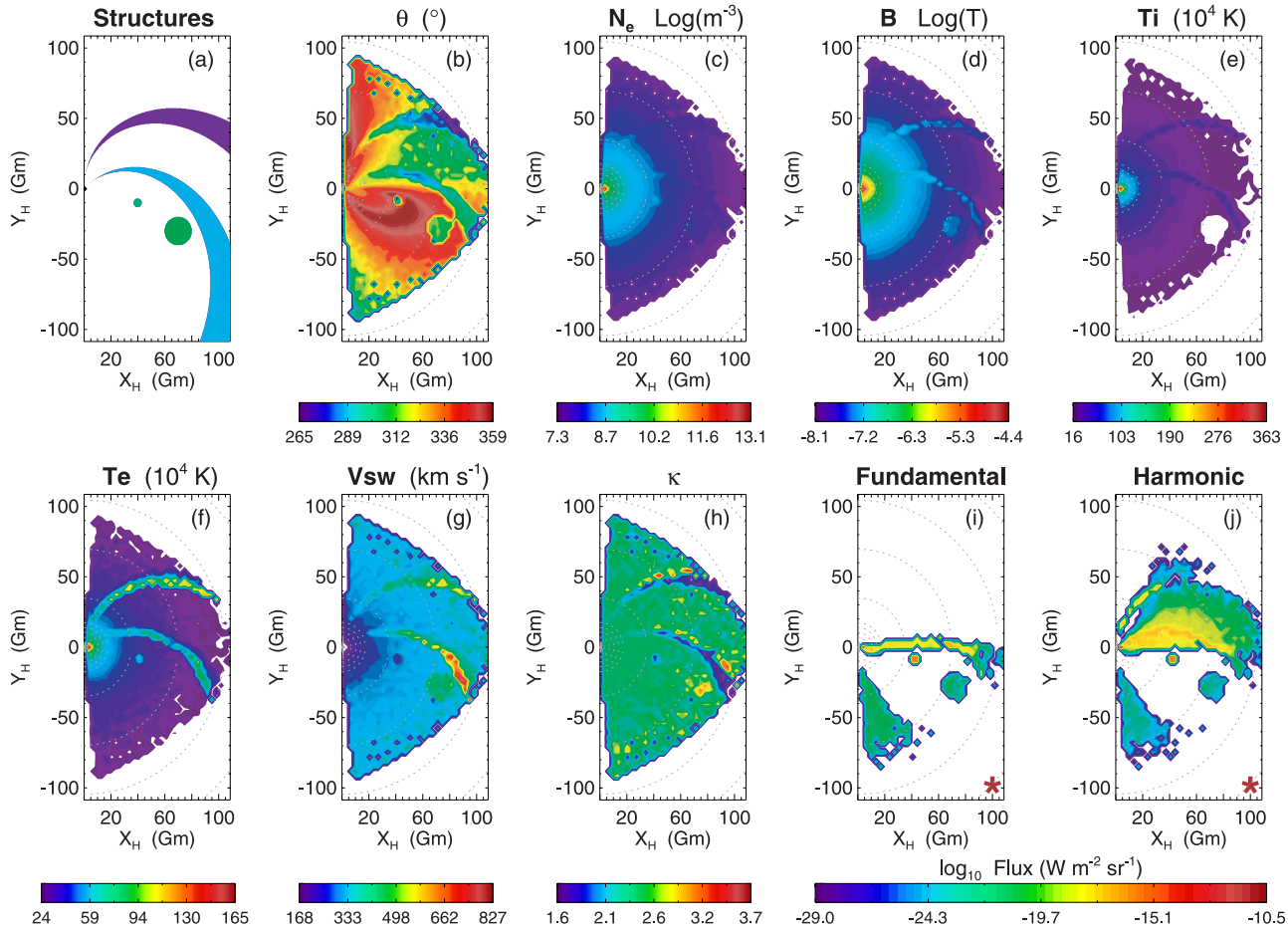


**Figure 8.** (a) Structures defined in the solar wind; (b) angle θ between the magnetic field and the global shock normal; (c) electron number density $N_e$; (d) magnetic field strength $B$; (e) ion temperature $T_i$; (f) electron temperature $T_e$; (g) solar wind speed $V_{sw}$; (h) level of nonthermal electrons, parameterized by κ; (i) received, frequency integrated, fundamental emission as a function of location; and (j) received, frequency integrated, harmonic emission as a function of location. The observer location is marked by an asterisk in Figures 8a and 8j.

that of the shock's leading edge, as for the harmonic emission. Here the clear difference between the temporal extents of the fundamental and harmonic emission bands emphasizes the dependence of dynamic spectra on observer location.

## 5. Discussion and Conclusions

[50] Here this paper's results are reviewed in the context of papers 1–3. The implications these results have for observational interpretations of type II bursts are then discussed.

### 5.1. Results of the Model

[51] It has been shown, in papers 1–3 as well as in this paper, that a considerable number of type II radio burst properties can be produced with a relatively simple theoretical model. In particular, the calculations in sections 3 and 4 show that the theoretical model can produce features strongly reminiscent of coronal and interplanetary observations [e.g., *Nelson and Melrose*, 1985; *Reiner et al.*, 1998; *Gopalswamy et al.*, 2001c], including (1) reasonable emission intensities for both fundamental and harmonic frequency bands; (2) both broad and narrow bandwidth emission; (3) type II-like frequency drift rates; and (4) shocks which produce emission below the detection threshold and thus appear radio quiet. Further, it has been found that predicted dynamic spectra can (1) be dominated by localized source regions; (2) be different for distinct observer locations, especially in the fundamental component; and (3) have frequency drift rates which depend not just on the shock speed but also on the relative motion of the source region with respect to the global shock, for example, due to lateral expansion, motion along a CIR or other structure, or other transverse motions relative to $\mathbf{V}_{shock}$. These calculations also support previous interpretations of interplanetary data in terms of interactions with of CIRs and preexisting CME material [*Reiner et al.*, 1998; *Gopalswamy et al.*, 2001c], multiple-lane events in terms of multiple emitting portions of a shock [*McLean*, 1985] and/or interactions with localized structures [*Reiner et al.*, 1998], and the effects on bandwidth of shock expansion and radial extent [*Weiss*, 1963]. While previous interpretations of split-bands in terms of upstream/downstream [*Smerd et al.*, 1974] or intrinsic

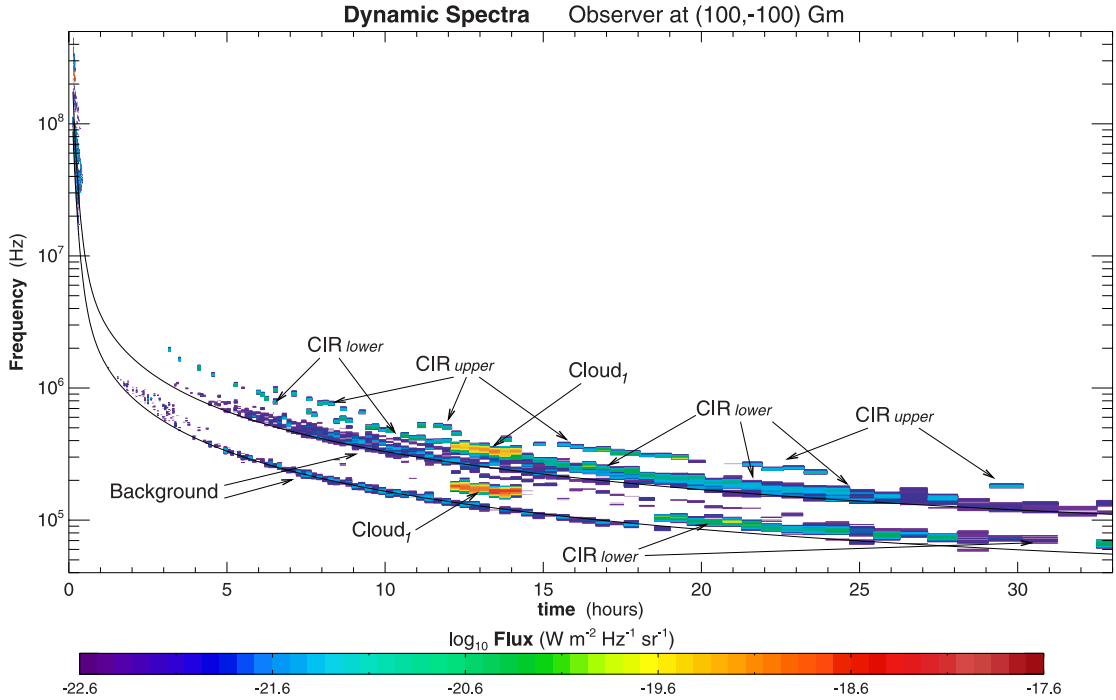


**Figure 9.** Dynamic spectrum of a type II burst. The two solid curves are the fundamental and harmonic frequency drift rate of the shock's leading edge. The structures responsible for various spectral features are indicated.

emission physics may be viable, Figure 7 suggests that split-bands may potentially result from a deficit of radiation resulting from a localized structure: Note that if the loop were colder and denser, then it might produce no observable emission.

[52] Whether or not type II emission will occur over the metric, DH, and kilometric wavelength ranges depends on the spatial profiles of $N_e$ and $B$, and subsequently $V_A$, as well as the time varying shock speed. If a peak is present in $V_A$ along the path of a type II emitting shock, then, provided $U \lesssim 2V_A$, it should be observable in its dynamic spectra. This potentially makes type II a useful further constraint on coronal $N_e$ and $B$ models.

[53] In the corona, rapidly expanding shocks can produce very broad emission bands. Narrowband emission in the corona requires localized emission sources. However, reducing the size of the source region generally reduces emission levels. Therefore, intense narrowband emission should most often be associated with localized structures which provide favorable conditions for emission. One notable consequence of the influence that $N_e$, $V_{sw}$, and magnetic field direction have on type II bursts is that emission should be more favorably produced by equatorial shocks than more poleward shocks, which would encounter the typically lower density fast solar wind.

[54] The ratio of fundamental to harmonic emission in a type II event can give insight into the underlying conditions. Fundamental emission at an observer can be significantly weaker due to either unfavorable source conditions or difficulty in the produced emission reaching the observer. Harmonic emission is considerably less affected by propagation difficulties, and is thus mostly modulated by source conditions.

[55] As well as the observed properties mentioned above, a useful quantification of the conditions relevant to type II emission has been built up. Specifically, the following conditions all prove favorable for emission: fast shocks (speed relative to the upstream plasma); large shocks; expanding shocks, particularly relevant in the corona; high upstream $T_e$; weak upstream $B$; $\theta_{UB} \sim 90°$ or equivalently 270°; high upstream $N_e$; and low upstream $\kappa$ (more nonthermal electrons). High $T_i$ acts to increase fundamental emission while decreasing harmonic emission.

### 5.2. Implications for Observational Interpretation

[56] It should be remembered that while individual characteristics, such as CME width and rate of expansion, are capable of strongly influencing the ability of a given driver to produce radio emission, no single parameter can describe all aspects relevant to the type II emission process. For example, a large fast (strong) shock can be radio poor if there are insufficient nonthermal electrons available to be reflected and accelerated, or if $\theta_{UB} \sim 0°$. Equivalently, a shock which produces electron beams can still fail to produce significant type II emission if parameters, such as $T_e$, which influence the growth of plasma waves and their conversion to radio emission, are unfavorable. Further, due to the variability in $V_A$ and $V_{sw}$ in time and space, it is possible for a disturbance traveling in a given direction at a given time to produce observable emission while an equivalent (speed, size) disturbance traveling in a different direction or at a different time can be radio quiet. What this all means is that one cannot expect to interpret type II

observations in detail while considering only a subset of the influencing factors.

[57] While investigations into the statistical relationships between one property, such as the size or the speed of a shock, and the associated occurrence of type II emission have been useful, it is fundamentally limited as a method of detailed interpretation due to the other aspects of the emission process being ignored. Only through detailed consideration of the many aspects of the emission, and the use of alternative (e.g., white light) determinations of source conditions, such as $N_e$, can conclusive observational relationships hope to be determined.

[58] Finally, the possibilities for inverting the results of this work, and thus determining the nature of coronal and solar wind structures based on observed type II spectra, are limited at present. The difficulty arises due to the potential for multiple combinations of plasma variables to produce similar levels of emission. Further, details of the global shock structure are currently very poorly constrained observationally and will probably remain so for the foreseeable future. However, despite these limitations, it is possible that when combined with the available observations, this theoretical model may be able to further constrain the type II source region and global shock structure. As an example, broadband emission in the absence of notable upstream density fluctuations is most likely dominated by the heliocentric extent of the type II source region, and as the source region is tied to the shock front the bandwidth can provide a constraint on the global shock structure.

[59] **Acknowledgments.** The authors thank P. A. Robinson for useful comments on this manuscript. We acknowledge financial support from the Australian Research Council.

[60] Shadia Rifai Habbal thanks A. Lara and another referee for their assistance in evaluating this paper.

## References

Bale, S. D., M. J. Reiner, J. L. Bougeret, M. L. Kaiser, S. Krucker, D. E. Larson, and R. P. Lin (1999), The source region of an interplanetary type II radio burst, *Geophys. Res. Lett.*, *26*, 1573.

Ball, L., and D. B. Melrose (2001), Shock drift acceleration of electrons, *Publ. Astron. Soc. Aust.*, *18*, 361.

Cairns, I. H. (1986), The source of free energy for type II solar radio bursts, *Proc. Astron. Soc. Aust.*, *6*, 444.

Cairns, I. H. (1987), The electron distribution function upstream from the Earths bow shock, *J. Geophys. Res.*, *92*, 2315.

Cairns, I. H. (1988), A semiquantitative theory for the $2f_p$ radiation observed upstream from the Earth's bow shock, *J. Geophys. Res.*, *93*, 3958.

Cairns, I. H., and P. A. Robinson (1997), First test of stochastic growth theory for the Langmuir waves in Earth's foreshock, *Geophys. Res. Lett.*, *24*, 369.

Cairns, I. H., and P. A. Robinson (1999), Strong evidence for stochastic growth of Langmuir-like waves in Earth's foreshock, *Phys. Rev. Lett.*, *82*, 3066.

Cairns, I. H., and R. D. Robinson (1987), Herringbone bursts associated with type II solar radio emission, *Solar Phys.*, *111*, 365.

Cairns, I. H., P. A. Robinson, and R. R. Anderson (2000), Thermal and driven stochastic growth of Langmuir waves in the solar wind and Earth's foreshock, *Geophys. Res. Lett.*, *27*, 61.

Cairns, I. H., S. A. Knock, P. A. Robinson, and Z. Kuncic (2003), Type II solar radio bursts: Theory and space weather implications, *Space Sci. Rev.*, *107*, 27.

Cairns, I. H., J. J. Mitchell, S. A. Knock, and P. A. Robinson (2004), Towards a quantitative theory for 2–3 kHz radio emission from beyond the heliopause, *Adv. Space Res.*, in press.

Collier, M. R., A. Szabo, J. A. Slavin, and R. P. Lepping (2000), IMF length scales and predictability: The two length scale medium, *Int. J. Geomagn. Aeron.*, *2*, 3.

Filbert, P. C., and P. J. Kellogg (1979), Electrostatic noise at the plasma frequency beyond the Earth's bow shock, *J. Geophys. Res.*, *84*, 1369.

Gopalswamy, N., A. Lara, S. Yashiro, M. L. Kaiser, and R. A. Howard (2001a), Predicting the 1-AU arrival times of coronal mass ejections, *J. Geophys. Res.*, *106*, 29,207.

Gopalswamy, N., A. Lara, M. L. Kaiser, and J.-L. Bougeret (2001b), Near-Sun and near-Earth manifestations of solar eruptions, *J. Geophys. Res.*, *106*, 25,261.

Gopalswamy, N., S. Yashiro, M. L. Kaiser, R. A. Howard, and J.-L. Bougeret (2001c), Radio signatures of coronal mass ejection interaction: Coronal mass ejection cannibalism?, *Astrophys. J.*, *548*, L91.

Hollweg, J. V., M. K. Bird, H. Volland, P. Edenhofer, C. T. Stelzried, and B. L. Seidel (1982), Possible evidence for coronal Alfvèn waves, *J. Geophys. Res.*, *87*, 1.

Holman, G. D., and M. E. Pesses (1983), Solar type II radio emission and the shock drift acceleration of electrons, *Astrophys. J.*, *267*, 837.

Knock, S. A., I. H. Cairns, P. A. Robinson, and Z. Kuncic (2001), Theory of type II radio emission from the foreshock of an interplanetary shock, *J. Geophys. Res.*, *106*(A11), 25041, doi:10.1029/2001JA000053.

Knock, S. A., I. H. Cairns, P. A. Robinson, and Z. Kuncic (2003a), Theoretically predicted properties of type II radio emission from an interplanetary foreshock, *J. Geophys. Res.*, *108*(A3), 1126, doi:10.1029/2002JA009508.

Knock, S. A., I. H. Cairns, and P. A. Robinson (2003b), Type II radio emission predictions: Multiple shock ripples and dynamic spectra, *J. Geophys. Res.*, *108*(A10), 1361, doi:10.1029/2003JA009960.

Kuncic, Z., I. H. Cairns, S. A. Knock, and P. A. Robinson (2002), A quantitative theory for terrestrial foreshock radio emission, *Geophys. Res. Lett.*, *29*(8), 1161, doi:10.1029/2001GL014524.

Mancuso, S., and S. R. Spangler (1999), Coronal Faraday rotation observations: Measurements and limits on plasma inhomogeneities, *Astrophys. J.*, *525*, 195.

Mann, G., H. Aurass, A. Klassen, C. Estel, and B. J. Thompson (1999), Coronal transient waves and coronal shock waves, in *Proceedings of the 8th SOHO Workshop*, *SP-446*, p. 477, Eur. Space Agency, Paris.

Mann, G., H. T. Classen, E. Keppler, and E. C. Roelof (2002), On electron acceleration at CIR related shock waves, *Astron. Astrophys.*, *391*, 749.

Mann, G., A. Klassen, H. Aurass, and H. T. Classen (2003), Formation and development of shock waves in the solar corona and the near-Sun interplanetary space, *Astron. Astrophys.*, *400*, 329.

McLean, D. J. (1985), Metrewave solar radio bursts, in *Solar Radiophysics: Studies of Emission From the Sun at Metre Wavelengths*, edited by D. J. McLean and N. R. Labrum, p. 37, Cambridge Univ. Press, New York.

Melrose, D. B. (1985), *Instabilities in Space and Laboratory Plasmas*, Cambridge Univ. Press, New York.

Mitchell, J. J., I. H. Cairns, and P. A. Robinson (2004), Theory for 2–3 kHz radiation from the outer heliosphere, *J. Geophys. Res.*, *109*, A06108, doi:10.1029/2003JA010117.

Nelson, G. J., and D. B. Melrose (1985), Type II bursts, in *Solar Radiophysics: Studies of Emission From the Sun at Metre Wavelengths*, edited by D. J. McLean and N. R. Labrum, p. 333, Cambridge Univ. Press, New York.

Newkirk, G., Jr. (1961), The solar corona in active regions and the thermal origin of the slowly varying component of solar radio radiation, *Astrophys. J.*, *133*, 983.

Reiner, M. J., M. L. Kaiser, J. Fainberg, J.-L. Bougeret, and R. G. Stone (1998), On the origin of radio emission associated with the January 6–11, 1997, CME, *Geophys. Res. Lett.*, *25*, 2493.

Roberts, J. A. (1959), Solar radio bursts of spectral type II, *Aust. J. Phys.*, *11*, 215.

Robinson, P. A. (1992), Clumpy Langmuir waves in type III solar radio sources, *Solar Phys.*, *139*, 147.

Robinson, P. A., and I. H. Cairns (1993), Stochastic growth theory of type III solar radio emission, *Astrophys. J.*, *418*, 506.

Robinson, P. A., and I. H. Cairns (1998), Fundamental and harmonic emission in type III solar radio bursts III: Heliocentric variations of interplanetary beam and source parameters, *Solar Phys.*, *181*, 429.

Robinson, P. A., I. H. Cairns, and D. A. Gurnett (1993), Clumpy Langmuir waves in type III radio sources: Comparison of stochastic-growth theory with observations, *Astrophys. J.*, *407*, 790.

Robinson, P. A., I. H. Cairns, and A. J. Willes (1994), Dynamics and efficiency of type III solar radio emission, *Astrophys. J.*, *422*, 870.

Saito, K., A. I. Poland, and R. H. Munro (1977), A study of the background corona near solar minimum, *Solar Phys.*, *57*, 121.

Smerd, S. F., K. V. Sheridan, and R. T. Stewart (1974), On split-band structure in type II radio burrsts from the Sun, in *Coronal Disturbances: Proceedings of the IAU Symposium*, vol. 57, edited by G. Newkirk, p. 389, Springer-Verlag, New York.

Toptyghin, I. N. (1980), Acceleration of particles by shocks in a cosmic plasma, *Space Sci. Rev.*, *26*, 157.
Webb, G. M., W. I. Axford, and T. Terasawa (1983), On the drift mechanism for energetic charged particles at shocks, *Astrophys. J.*, *270*, 537.
Weiss, A. A. (1963), The positions and movements of sources of solar radio bursts of spectral type II, *Aust. J. Phys.*, *16*, 240.
Wu, C. S. (1984), A fast Fermi process: Energetic electrons accelerated by a nearly perpendicular bow shock, *J. Geophys. Res.*, *89*, 8857.

I. H. Cairns and S. A. Knock, School of Physics, A28, University of Sydney, NSW 2006, Australia. (sknock@physics.usyd.edu.au)